

Cuprate high- T_c superconductors

In solid-state physics two different paradigms are typically applied. The first is a local picture, in which one visualizes the quantum states of electrons in atomic orbitals or at impurity atoms in real space (r -space). The second is the momentum or reciprocal space (k -space) picture, where electrons are viewed as de Broglie waves completely delocalized throughout the material. Understanding these two separate paradigms is essential for a complete understanding of the physics of condensed matter, but rarely has it been as necessary to combine both pictures as it has been to gain insight into the electronic structure of the high-temperature superconductors (HTSCs). In this article, we review recent developments in the understanding of the relationship between the r -space and k -space electronic spectroscopies used to explore high-temperature superconductivity.

Kyle M. Shen and J. C. Seamus Davis

LASSP, Department of Physics, Cornell University, Ithaca, NY 14850, USA

E-mail: kmshe@cornell.edu, jcdavis@ccmr.cornell.edu

The classic Bardeen–Cooper–Schrieffer (BCS) theory of superconductivity from 1957 is founded upon the k -space paradigm. Here attractive electron–electron interactions between states of opposite spin and k result in the formation of Cooper pairs – spin-zero bound states of the two electrons. A fluid of delocalized Cooper pairs forms the basis of superconductivity, with dissipationless electrical transport protected by an energy gap Δ , where 2Δ is the energy needed to break apart a Cooper pair. For classical superconductors, the ‘coherence’ length, or the approximate spatial extent of a Cooper pair, is usually hundreds

of nanometers, so that these paired states average over any perturbation at the atomic level, making the r -space picture largely irrelevant.

High-temperature superconductivity in cuprates is dramatically different. These materials are comprised of one or more crystal planes per unit cell consisting of only Cu and O atoms in a square lattice. Superconductivity originates among the strongly interacting electrons in these CuO_2 planes. In the absence of holes, the so-called parent compounds have an antiferromagnetic Mott insulating ground state in which Coulomb repulsion prevents electron hopping from Cu to

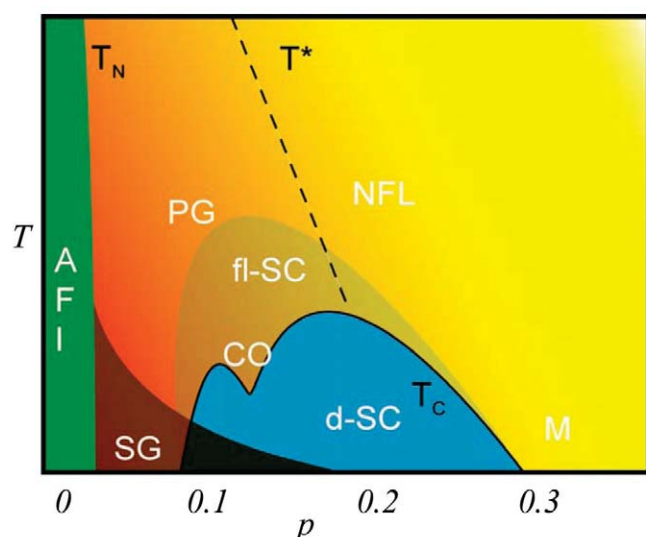


Fig. 1 Schematic phase diagram of the hole-doped cuprates as a function of temperature (T) and hole doping (p). AFI refers to the antiferromagnetic insulator, PG the pseudogap regime, d-SC the d-wave superconductor, M the metallic state, NFL the non-Fermi liquid state, SG the spin glass regime, and CO the charge-ordered state.

Cu and the exchange correlation is antiferromagnetic in sign. Doping these insulating CuO_2 layers with holes (removing electrons) causes the appearance of new electronic ordered states including high-temperature superconductivity. A schematic phase diagram of hole-doped cuprates is shown in Fig. 1. The maximum critical temperatures (T_c) of up to 145 K occur at an optimal hole-doping near $p \sim 0.16$ where p is the number of doped holes per Cu atom.

One of the defining characteristics of the HTSCs is the strong momentum k (or directional) dependence of their electronic properties. Nowhere is this better illustrated than in the $d_{x^2-y^2}$ symmetry of the superconducting order parameter – that is to say, the superconducting electrons are paired strongly for k parallel to the Cu–O–Cu bond directions, but not paired at all for k along the diagonals of the square lattice, resulting in many profound implications. However, r -space is also critical for cuprates. They exhibit coherence lengths in the nanometer range, meaning that the Cooper-pair wavefunctions

cannot average over atomic-scale disorder. Moreover almost all are, by nature, nonstoichiometric compounds. In order to realize exotic emergent properties such as superconductivity, it is necessary to chemically substitute or intercalate atoms at a concentration level of $\sim 10\%$, many orders of magnitude greater than what is found in typical semiconductors. These extremely high doping levels imply that the HTSCs are very disordered at the atomic scale in r -space. Finally, there is growing evidence that intrinsic spatial variations in the electronic and superconducting properties may play a key role to understanding the nature of high-temperature superconductivity^{1–5}.

To understand the pairing mechanism and phase diagram of cuprate HTSCs and to develop a predictive theory to be used in the search for new, even higher T_c superconductors, the excited-state electronic structure must be understood in both r -space and in k -space. These excited states can be studied with great precision by two closely related single-particle spectroscopies: angle-resolved photoemission spectroscopy (ARPES) and spectroscopic imaging scanning tunneling microscopy (SI-STM).

ARPES

To date, the premier tool for the direct study of the k -space dependence of electronic properties is ARPES, which uses a high-intensity beam of ultraviolet or X-ray photons to illuminate a sample. An electron spectrometer then analyzes the outgoing kinetic energies and directions of the photoelectrons, allowing a determination of the initial quantum states of the electrons within the solid (Fig. 2). For a comprehensive overview of photoemission spectroscopy, see Hüfner⁶, and for a review of photoemission studies of the cuprate superconductors see Damascelli *et al.*⁷.

The power of ARPES stems from its capacity to directly extract the electrons' energy and momentum states. This also provides information about the types of interactions that the electrons experience within the solid, making it an ideal tool for studying materials such as HTSCs, in which the effects of quantum many-body interactions are paramount. However, it is a spatially averaged probe, typically over the millimeter scale, which can pose an issue for

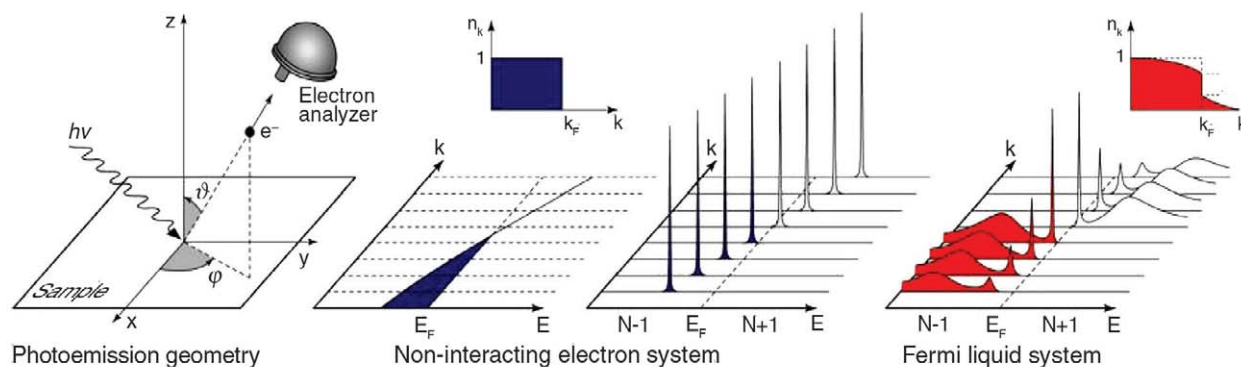


Fig. 2 Schematic representation of ARPES (far left). Extraction of the physical data and relationship to the density of states as a function of momentum and the single-particle excitation spectra. (Reproduced with permission from⁷. © 2003 American Physical Society.)

materials where atomic-scale variations play an important role in the underlying physics.

SI-STM

SI-STM has undergone rapid development in order to allow the r -space electronic structure of cuprates to be studied. For example, energy-resolved local density of states (LDOS) imaging⁸ in which measurements of the STM tip-sample differential tunneling conductance $g(\vec{r}, V) \equiv dI/dV_{\vec{r}, V}$ at grid locations \vec{r} and sample bias voltage V , yield a spatial image proportional to the local density of electronic states, $LDOS(\vec{r}, E)$, at energy E . The resulting *gap-map* technique^{1,2,5,9} images superconducting energy-gap variations $\Delta(\vec{r})$ with atomic resolution by measuring the peak-to-peak energy separation in a typical spectrum. A third technique is Fourier transform scanning tunneling spectroscopy (FT-STS)^{10,11} in which the \vec{q} -vectors of spatial modulations in $g(\vec{r}, E)$ are determined from the locations of peaks in $g(\vec{q}, E)$, the Fourier transform magnitude of $g(\vec{r}, E)$, and used to determine elements of the k -space electronic structure.

Materials

In this paper we discuss two canonical cuprates: $\text{Ca}_{2-x}\text{Na}_x\text{CuO}_2\text{Cl}_2$ (Na-CCOC) and $\text{Bi}_2\text{Sr}_2\text{CaCu}_2\text{O}_{8+\delta}$ (Bi-2212). They have completely different crystallographic structures, chemical constituents, and dopant species/sites in the termination layers lying between the CuO_2 plane and vacuum. Na-CCOC has a single CuO_2 layer capped by a perfectly square ionic CaCl layer, with Na dopant atoms substituted at the Ca site. Bi-2212 has a CuO_2 bilayer, above which are both BiO and SrO layers whose unit cells experience an incommensurate crystal supermodulation; non-stoichiometric oxygen dopant atoms are located

interstitially near the BiO layer. Both cleave to reveal excellent surfaces for ARPES and SI-STM studies, and thus the vast majority of data for comparison between these techniques emerges from these materials. Despite their structural and chemical differences, the information discussed in this paper is consistent between the two families, indicating that our studies are probing the intrinsic properties of their only common feature – the CuO_2 planes.

Basic features of cuprate electronic structure from ARPES and SI-STM

The low-energy electronic features of these HTSCs can be classified into three main categories: (i) the quasiparticle states close to the d -wave node ($|E| < 30$ meV); (ii) the states around the superconducting gap maximum near the antinodes ($30 < |E| < 80$ meV); and (iii) the states at high energies ($|E| > 80$ meV), which reflect the effects of electron-boson interactions (EBIs). These energy ranges are shown as (i) purple, (ii) red, and (iii) green boxes in Fig. 3a and Fig. 4b. This article will review the contributions of ARPES and SI-STM in elucidating the nature of the electronic states in each of these three regimes.

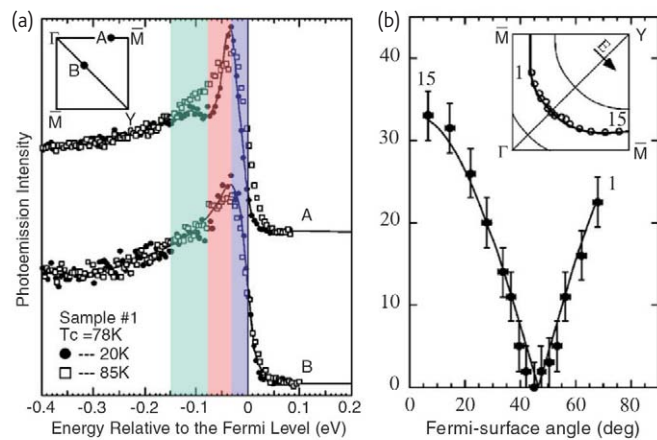


Fig. 3 (a) ARPES spectra of the antinodal (A) and nodal (B) states as a function of temperature. The three energy scales relating to (i) the nodal quasiparticles ($|E| < 30$ meV); (ii) the superconducting gap states ($30 < |E| < 80$ meV); and (iii) the high-energy states ($|E| > 80$ meV) are shown in purple, red, and green, respectively. (Reproduced with permission from¹², © 1993 American Physical Society.) (b) Anisotropy of superconducting gap around the Fermi surface, showing the $d_{x^2-y^2}$ symmetry, as measured by Ding et al.¹³.

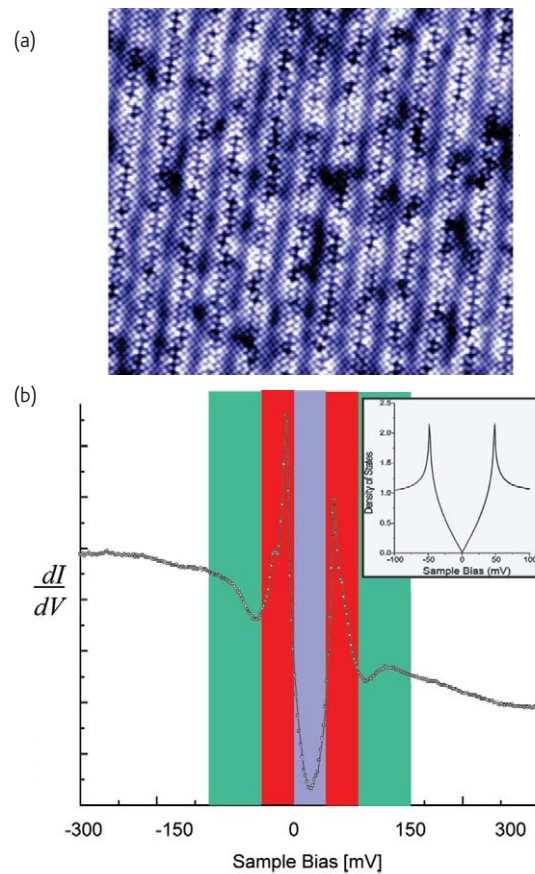


Fig. 4 (a) 25 nm square topographic image of the BiO surface of Bi-2212. (b) Typical differential conductance spectrum at $T = 4.2$ K showing the equivalent three energy ranges, i.e. (i) $|E| < 30$ meV in purple, (ii) $30 \text{ meV} < |E| < 80$ meV in red, (iii) $|E| > 80$ meV in green, as those discussed in Fig. 3. Inset shows a textbook d -wave BCS $DOS(E)$ spectrum.

Low-energy ‘nodal’ states: quasiparticle interference and AC ARPES

As mentioned above, one of the unique aspects of these HTSCs is the presence of a node in the superconducting order parameter, resulting in the fact that single-electron states can be excited with negligible energies, even down to zero temperature. The presence of these low-lying states is observed in ARPES as a group of well-defined and long-lived quasiparticle excitations along the zone diagonal which have a small or zero energy gap (corresponding to angles around 45° in Fig. 3b). These states have vast implications on the electronic and thermodynamic properties of these HTSCs, as evidenced in measurements of the specific heat, thermal conductivity, and transport measurements.

Remarkably, these states are also detectable by SI-STM. Due to the presence of the atomic-scale disorder, elastic scattering mixes momentum eigenstates at \vec{k}_1 and \vec{k}_2 , resulting in a quasiparticle interference (QPI) pattern with wavevector $\vec{q} = \vec{k}_2 - \vec{k}_1$. These interference phenomena can be observed by SI-STM as modulations of the differential tunneling conductance with wavelength $\lambda = 2\pi/|\vec{q}|$. When modulations in the LDOS are detected by SI-STM, certain contours in \vec{k} -space can be reconstructed by analyzing the Fourier transform of the real-space LDOS(E) image, a technique known as FT-STs^{14–17}. The set of 16 inequivalent interference modulations from FT-STs, $\vec{q} = \vec{k}_2 - \vec{k}_1$, have been successfully analyzed within a QPI model (Fig 5a), and found to agree quantitatively with ARPES measurements of the momentum and energies of the

quasiparticle states around the node, thereby yielding the position of the underlying Fermi surface as well as the detailed momentum-space structure of the superconducting energy gap $\Delta(\theta_k)$. A typical Fourier transform image is shown in Fig. 5b. These procedures are remarkably successful near optimal doping. In Bi-2212 as well as Na-CCOC, FT-STs yields measurements of the Fermi surface and $\Delta(\theta_k)$ that are consistent with ARPES.

Important studies using ARPES^{18–20} have also directly demonstrated that the above interpretation of FT-STs is, in fact, largely correct. By taking the autocorrelation of the ARPES data, one obtains the set of QPI wavevectors determined independently by FT-STs (Fig. 6). The self-consistency of the k -space phenomenology of the QPI model from both ARPES and FT-STs can now provide mutual confidence in the two techniques and unprecedented detailed information about the structure of the momentum structure of the superconducting gap that would not have been possible without the combination of data from both FT-STs and ARPES.

High-energy ‘antinodal’ states: real-space and momentum-space

Having discussed the agreement between SI-STM and ARPES for the low-energy electronic structure studies around the superconducting d -wave node, we now traverse along the Fermi surface towards the Brillouin zone boundary. At these locations in momentum space, we probe the so-called antinodal states where the energy gap is maximal. These antinodal states can be directly related to the high-energy

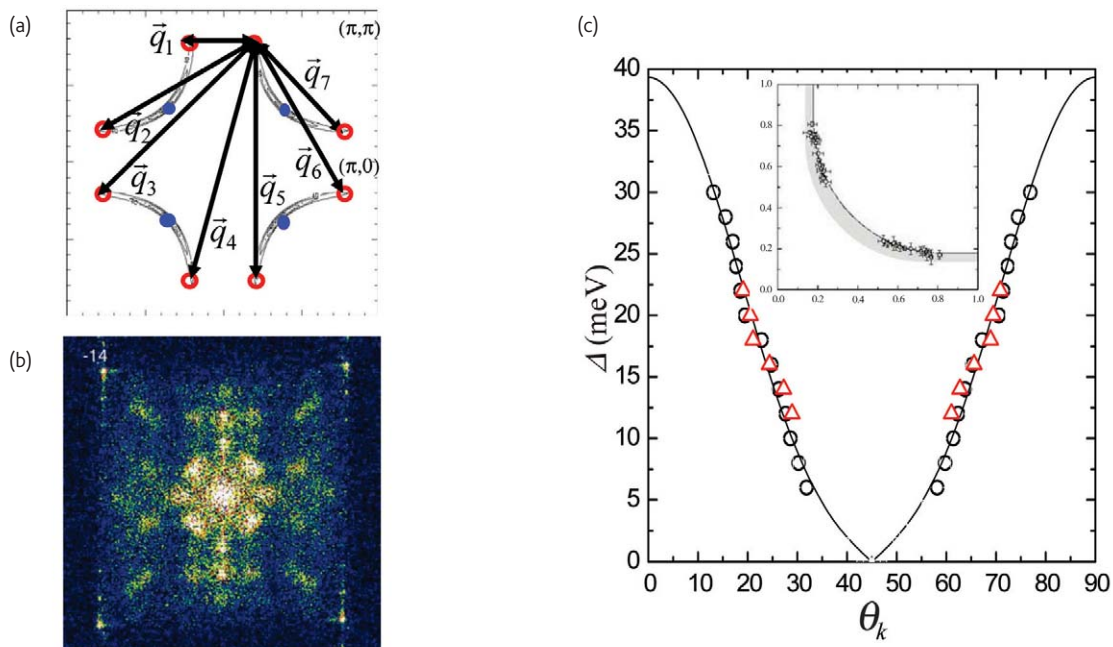


Fig. 5 Quasiparticle interference model. (a) Wavevectors connecting points of high DOS on the Fermi surface (blue). (b) A typical Fourier transform of a real-space LDOS image; $g(q, E = -14 \text{ meV})$. (c) The locus of scattering from FT-STs and Fermi-surface (grey) from ARPES is inset into the k -space structure of the superconducting energy gap $\Delta(\theta_k)$ derived only from r -space SI-STM data.

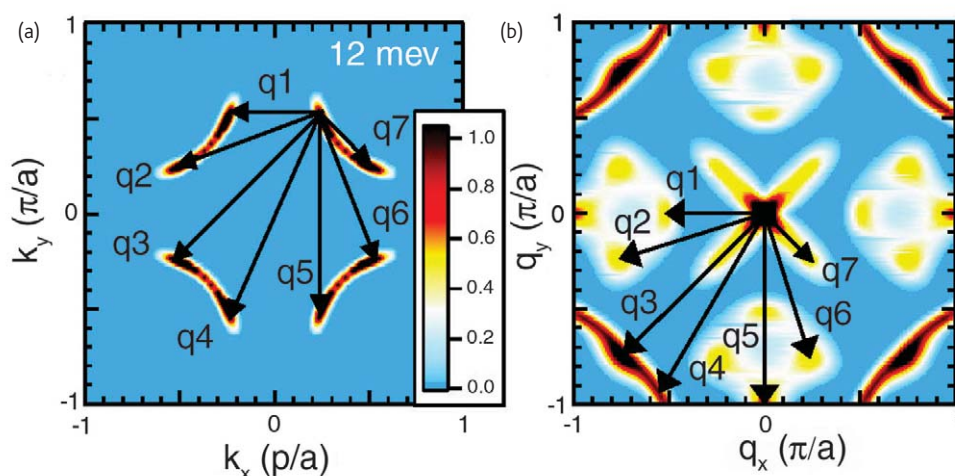


Fig. 6 (a) Quasiparticle interference model: wavevectors connecting points of high DOS in the ARPES-derived data. (b) The autocorrelation of (a) showing that the set of q -vectors of the FT-STs model is in fact observed directly. (Reproduced with permission from¹⁸. © 2006 American Physical Society.)

states (Fig. 4) measured by SI-STM due to their large density of states at these corresponding energies. At and above the optimal hole-doping level in the superconducting state, well-defined quasiparticle excitations are observed near the antinodes, and the QPI model can be applied successfully to describe the electronic states near the antinodes. However, below optimal doping, the situation becomes much more complex.

Here the electronic excitations along the antinodal directions become very heavily scattered with extremely short lifetimes, and no well-defined quasiparticle excitations can be observed in those regions of k -space. This can also be observed in the momentum-space maps of the low-energy excitations as measured by ARPES by measuring spectra throughout the Brillouin zone and integrating a narrow energy window around E_F (typically ± 10 meV). Momentum-space Fermi energy maps produced in this fashion are shown in Fig. 7. A striking feature of these maps is that the intensity is strongly concentrated along the $(0,0)$ – (π,π) directions, and drops off precipitously near the antinodes, forming a discontinuous, arc-like feature. This suppression of intensity is a clear signature of the lack of well-defined QPs near

the antinodes, and this suppression of intensity can persist up to high energies (~ 100 meV) as seen in Fig. 8.

Comparison of the ARPES data with SI-STM studies reveals a simple explanation for why the antinodal states appear so incoherent in k -space when measured by ARPES. At hole densities $p < 14\%$, the electronic structure appears static in r -space and independent of E for higher energies. In fact, it consists of the atomic-scale spatial patterns first reported by Kohsaka *et al.*²² but is now²³ identifiable as the pseudogap excitations at $E = \pm\Delta_1$. The low p antinodal excitations, which comprise these higher-energy states, locally break the translational symmetry, and reduce the C_4 rotational symmetry of electronic structure in each Cu plaquette to C_2 in Cu–O–Cu bond-centered patterns without long-range order (Fig. 9). Thus the antinodal states are quasilocized in r -space (probably by a combination of intrinsic inelastic scattering⁵ at low p , and dopant disorder²⁴) and cannot therefore be well defined in k -space. Moreover, this bond-centered electronic structure which breaks C_4 symmetry down to C_2 symmetry on each plaquette is not inconsistent with localized d -wave singlets.

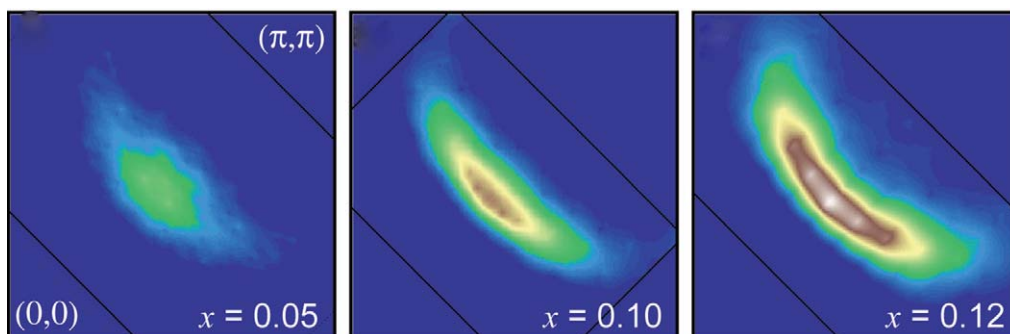


Fig. 7 Momentum-space map of intensity in a narrow window (± 10 meV) around the Fermi energy for different hole concentrations of $\text{Ca}_{2-x}\text{Na}_x\text{CuO}_2\text{Cl}_2$, showing the arc-like feature and suppressed spectral intensity near the antinodes (zone boundary). (Reproduced with permission from²¹. © 2005 American Association for the Advancement of Science.)

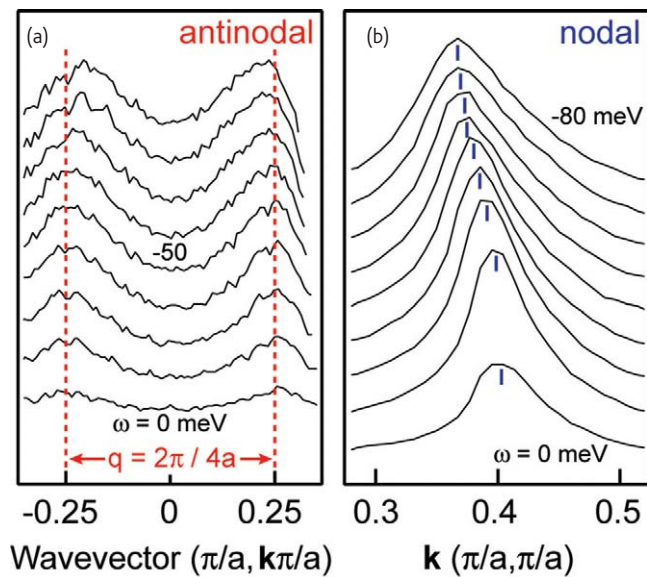


Fig. 8 Cuts of intensity at different energies along the antinodal (A) and nodal (B) directions, demonstrating the presence of well-defined, dispersive quasiparticle excitations along the nodal direction, and the lack of coherent quasiparticle states around the antinodes. (Reproduced with permission from²¹. © 2005 American Association for the Advancement of Science.)

Electron–boson interactions

Finally we discuss the high-energy states for $|E| > \Delta$. Here we are primarily dealing with energy states associated with EBI. The first observation of electron–lattice interactions via electron tunneling measurements was a critical development in the confirmation of the BCS theory of superconductivity, where single electrons form a

Cooper pair through the exchange of virtual phonons. The search for an analogous pairing boson or ‘glue’ for these HTSCs takes us to the third energy scale, which has recently been investigated by both ARPES and SI-STM measurements.

Given the ability of ARPES to probe the interactions experienced by the electrons, it should, in principle, be a natural technique for observing any ‘pairing glue’, or EBI, which holds together the superconducting Cooper pairs. The EBI manifest themselves as ‘breaks’ or ‘kinks’ in the quasiparticle dispersion near the corresponding energy of the boson, as measured in the ARPES spectra, and shown in model systems with strong electron–phonon interactions such as Be(0001)²⁵ or Mo(110)²⁶ (Fig. 10).

The presence of strong EBI in the ARPES spectra was first identified in the cuprates by Bogdanov *et al.*²⁷ and by Kaminski *et al.*²⁸. By fitting a pair of straight lines to the measured quasiparticle dispersion (a line at higher binding energies below the kink, and another at lower binding energies above the kink), one can produce estimates for the boson energy (the energy position of the kink) and the coupling strength (the ratio between the slopes of the two lines: $s_{\text{high}}/s_{\text{low}} = \lambda + 1$, where λ is the coupling constant). For an optimally doped sample of Bi2212 along the nodal direction, this analysis yielded values of $\omega_0 \sim 70$ meV and $\lambda \sim 1$ (Fig. 10b).

Later work by Lanzara *et al.*²⁹ proposed that the nature of the boson was a lattice vibration (or optical phonon) associated with the motions of the in-plane oxygen atoms. This argument was based on the fact that the energy of the boson as measured by ARPES remains largely independent of doping or material family (Fig. 10a–c), while the energy scales associated with superconducting features can vary dramatically

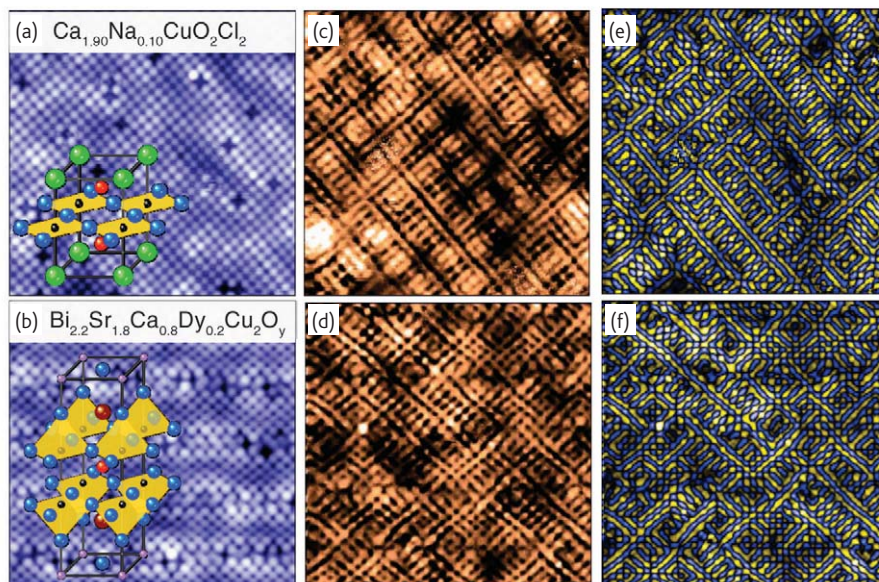


Fig. 9 (a, b) Topographic images of $\text{Ca}_{1.90}\text{Na}_{0.10}\text{CuO}_2\text{Cl}_2$ and $\text{Bi}_{2.2}\text{Sr}_{1.8}\text{Ca}_{0.8}\text{Dy}_{0.2}\text{Cu}_2\text{O}_y$ surfaces, respectively. (c, d) Simultaneous electronic structure images from SI-STM revealing the spatial structure of the antinodal or pseudogap excitations breaking translational symmetry, and reducing the C_4 rotational symmetry of the electronic structure in each Cu plaquette to C_2 in Cu–O–Cu bond-centered patterns without long-range order. (e, f) Laplacian filters of (c) and (d) to make the bond-centered C_2 contrast even clearer.

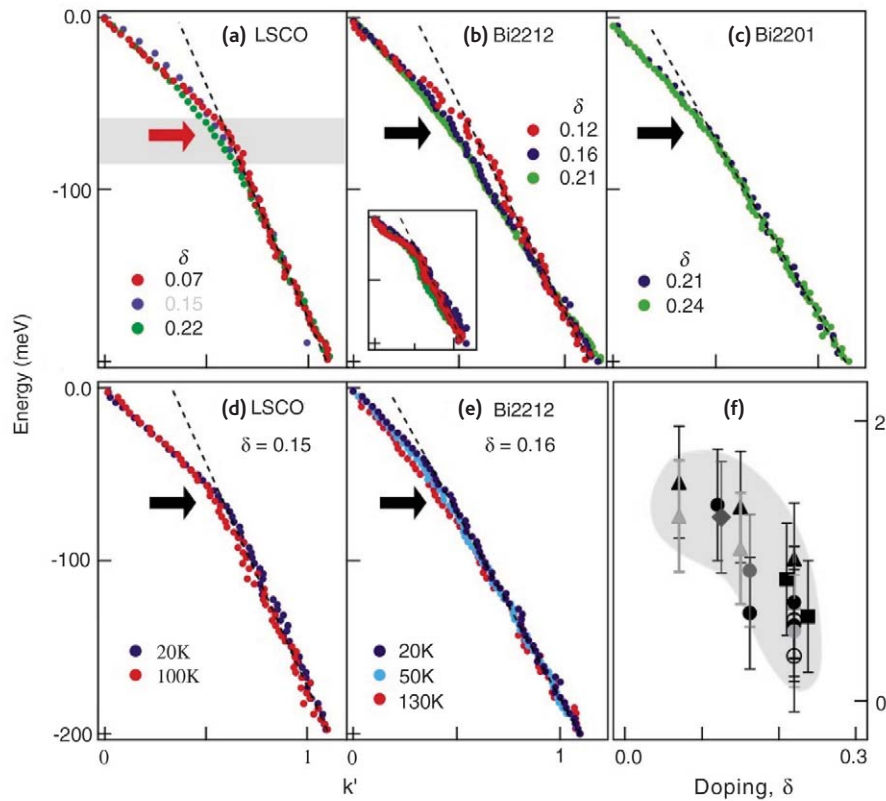


Fig. 10 Quasiparticle dispersions along the nodal direction as measured by ARPES in a series of cuprates: (a) $\text{La}_{2-x}\text{Sr}_x\text{CuO}_4$, (b) $\text{Bi}_2\text{Sr}_2\text{CaCu}_2\text{O}_{8+d}$, (c) $\text{Bi}_2\text{Sr}_2\text{CuO}_{6+d}$, showing a clear 'kink' or break in the dispersion around 70 meV. The existence and position of the kink appears to be largely temperature independent (d, e), while the estimated coupling appears to increase towards lower hole doping levels (f). (Reproduced with permission from²⁹. © 2001 Nature Publishing Group.)

as a function of carrier doping or material composition. Further ARPES work has studied the EBI in detail as a function of both momentum and carrier concentration. However, this interpretation still remains an open topic of debate, as other groups have argued that the EBI observed in ARPES originates from the interactions between electrons and spin excitations^{28,30,31}. In fact, the very necessity of a pairing boson for the superconducting state remains a contentious theoretical issue in the field of high-temperature superconductivity³².

Tunneling spectroscopy is also famous for its ability to interrogate the electron–boson coupling supporting superconductivity. The strong coupling theory of superconductivity predicts the impact of EBI on the superconducting $\text{DOS}(E)$ at energy $E = \Delta + \Omega$, where Δ is the superconducting energy gap and Ω is the boson energy. In fact, d^2I/dV^2 measurements on planar normal–insulator–superconductor tunnel junctions have been used to reveal these signatures at boson energies $\Omega = E - \Delta$, identifying them with independently determined phonons of energy Ω .

In cuprates, these phenomena can be detected at $E > \Delta$ in the LDOS in the region colored green in Figs. 3 and 4. Then $dI/dV(\vec{r}, E=eV)$ and $d^2I/d^2V(\vec{r}, E=eV)$ are simultaneously imaged with atomic resolution and register. From the former, the gapmap $\Delta(\vec{r})$ is derived, while, from the latter, the energies $\Pi(\vec{r})$ at which $d^2I/dV^2(\vec{r}, E)$ peaks

occur are measured and the boson interaction energy maps $\Omega(\vec{r}) = \Pi(\vec{r}) - \Delta(\vec{r})$ are then calculated. Such d^2I/dV^2 -signatures were studied for $p \sim 0.12 \rightarrow p \sim 0.24$. Histograms of Δ and Ω measured on five samples at different dopings reveal that, while the distributions of Δ evolve rapidly with doping, those of Ω appear unchanged: $\bar{\Omega} = 52 \pm 1 \text{ meV}$ for all dopings, showing that the above hypothesis is valid.

Finally, to test the hypothesis that the features in d^2I/dV^2 imaging are related to lattice vibration modes, crystals were prepared in which the normal ^{16}O was completely substituted by ^{18}O (as verified by frequency shifts detected in Raman spectroscopy). For each sample, the $\Delta(\vec{r})$ and $\Omega(\vec{r})$ are used to construct a two-dimensional histogram of the frequency of occurrence of spectra with a given pair of values (Δ, Ω) as shown in Fig. 11. Each histogram has a peak on the vertical axis at the most common gap energy $\bar{\Delta}$ and on the horizontal axis at the most common boson energy $\bar{\Omega}$. Comparison between ^{16}O Δ : Ω histogram (blue) and the ^{18}O Δ : Ω histogram (red) reveals immediately that, for any particular value of Δ , the value of Ω_0 for ^{18}O shifts downwards by approximately $3.5 \pm 1 \text{ meV}$ compared to that of ^{16}O . Consequently, substitution of ^{18}O for ^{16}O reduces the mean boson energy scale $\bar{\Omega}$ of EBI by $6\% (\approx 1 - \sqrt{16/18})$ as expected for lattice vibrational modes involving the O atom. This represented the

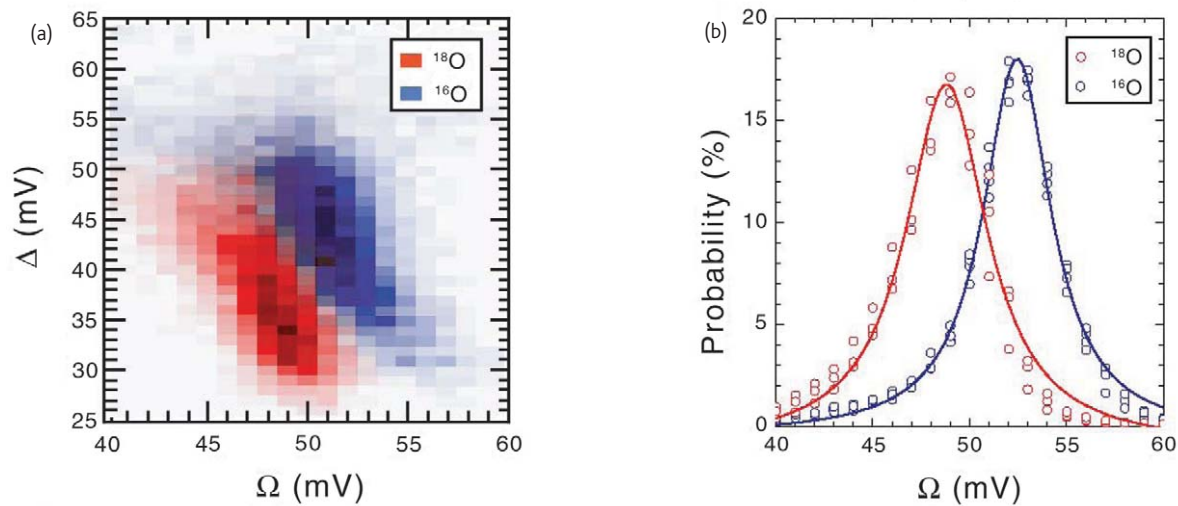



Fig. 11 (a) Joint histograms of Ω and Δ for ^{16}O and the ^{18}O showing the isotope shift in the mode energy. (b) The equivalent data plotting the histogram of Ω only.

first direct evidence for the effect of electron–lattice interaction on the electronic structure of cuprate superconductivity; this effect has recently been confirmed by ARPES³³.

Conclusions

The dual nature of the electronic structure of these cuprates has resulted in properties that cannot be understood from solely a real-space probe, or a momentum-space probe. As we have shown throughout this article, a complete understanding of the electronic quantum states that comprise these HTSCs can only come about through the powerful combination of both real and momentum space spectroscopies. In order to resolve many of the remaining challenges in high-temperature superconductivity, it may be necessary to develop an even more sophisticated methodology for integrating the information extracted from SI-STM and ARPES. A

key challenge is to find a spectral function $A(k, \omega)$ fully consistent with every detail of the electronic structure shown in Figs. 3 and 4. Finally, in addition to the HTSC cuprates, we believe that utilizing a similar approach will be essential to understanding many other families of complex electronic materials, especially the transition metal oxides, where the underlying physics depends both on momentum space anisotropy, and spatial variations on the atomic scale. 

Acknowledgments

We wish to acknowledge and thank our collaborators Hiroshi Eisaki, Dunghai Lee, Z.-X. Shen, Hidenori Takagi, Shin-ichi Uchida, J. Hoffman, Jinho Lee, Y. Kohsaka, K. McElroy, E. W. Hudson, V. Madhavan, and G. A. Sawatzky. This work has been supported by the Department of Energy, the Cornell Center for Materials Research funded by the National Science Foundation, and by a Grant-in-Aid for Scientific Research on Priority Area by a COE Grant from the Ministry of Education (Japan) and by a grant from NEDO (Japan).

REFERENCES

- Lang, K. M., et al., *Nature* (2002) **415**, 412
- Hoffman, J. E., et al., *Science* (2002) **266**, 455
- Lee, J., et al., *Nature* (2006) **442**, 546
- Kohsaka, Y., et al., *Science* (2007) **315**, 1380
- Allredge, J., et al., *Nat. Phys.* (2008) **4**, 319
- Hüfner, S., *Photoelectron Spectroscopy*, 3rd edition, Springer Verlag, Berlin, (2003)
- Damascelli, A., et al., *Rev. Mod. Phys.* (2003) **75**, 473
- Hudson, E. W., et al., *Science* (1999) **285**, 88
- Madhavan, V. et al., *Bull. Am. Phys. Soc.* (2000) **45**, 416
- Hoffman, J., et al., *Science* (2002) **297**, 1148
- McElroy, K., et al., *Nature* (2003) **422**, 520
- Shen, Z.-X., et al., *Phys. Rev. Lett.* (1993) **70**, 1553
- Ding, H., et al., *Phys. Rev. B* (1996) **54**, R9678
- Wang, Q.-H., and Lee, D.-H., *Phys. Rev. B* (2003) **67**, 020511
- Capriotti, L., et al., *Phys. Rev. B* (2003) **68**, 014508
- Nunner, T. S., et al., *Phys. Rev. B* (2006) **73**, 104511
- Hanaguri, T., et al., *Nat. Phys.* (2007) **3**, 865
- Chatterjee, U., et al., *Phys. Rev. Lett.* (2006) **96**, 107006
- Chatterjee, U., et al., *Phys. Rev. B* (2007) **76**, 012504
- McElroy, K., et al., *Phys. Rev. Lett.* (2006) **96**, 067005
- Shen, K. M., et al., *Science* (2005) **307**, 901
- Kohsaka, Y., et al., *Science* (2007) **315**, 1380
- Kohsaka, Y., et al., unpublished data
- McElroy, K., *Science* (2005) **309**, 1048
- Hengsberger, M. et al., *Phys. Rev. B* (1999) **60**, 10796
- Valla, T., et al., *Phys. Rev. Lett.* (1999) **83**, 2085
- Bogdanov, P. V., et al., *Phys. Rev. Lett.* (2000) **85**, 2581
- Kaminski, A., et al., *Phys. Rev. Lett.* (2001) **86**, 1070
- Lanzara, A., et al., *Nature* (2001) **412**, 510
- Borisenko, S. V., et al., *Phys. Rev. Lett.* (2003) **90**, 207001
- Johnson, P. D., et al., *Phys. Rev. Lett.* (2001) **87**, 177007
- Anderson, P. W., *Science* (2007) **317**, 1705
- Iwasawa, H., et al., unpublished data